Cooperative Sub-Millisecond Folding Kinetics of Apomyoglobin pH 4 Intermediate[†]

Sebastien Weisbuch, Francine Gérard, Marielle Pasdeloup, Jéremy Cappadoro, Yves Dupont, and Marc Jamin*

Laboratoire de Biophysique Moléculaire et Cellulaire, Université Joseph Fourier, BMC/DRDC, 17 rue des Martyrs, 38054 Grenoble Cedex 9, France

Received December 15, 2004; Revised Manuscript Received March 8, 2005

ABSTRACT: For small single-domain proteins, formation of the native conformation (N) from a fully unfolded form (U) or from a partially folded intermediate (I) occurs typically in a highly cooperative process that can be described by a two-state model. However, it is not clear whether cooperativity arises early along the folding reaction and whether folding intermediates are also formed in highly cooperative processes. Here, we show that each previously identified step leading apomyoglobin from its unfolded form to its native form, namely, the U ⇌ I_a, the I_a ⇌ I_b, and the I_b ⇌ N reactions, exhibits typical features of a two-state reaction. First, refolding and unfolding kinetics of the earliest U ⇌ I_a reaction are measurable at pH 4.2 within the urea-induced unfolding transition [Jamin, M., and Baldwin, R. L. (1996) *Nat. Struct. Biol. 3*, 613−618; Jamin, M., and Baldwin, R. L. (1998) *J. Mol. Biol. 276*, 491−504], and we report here that sub-millisecond kinetics measured by far-UV circular dichroism (CD), a probe of secondary structure, are similar to those measured by Trp fluorescence, a probe of hydrophobic core formation and chain collapse. These results confirm that folding of the earliest intermediate, I_a, occurs in a highly cooperative process, in which hydrophobic collapse and secondary structure formation occur concomitantly in the A(B)GH core. Second, when the refolding of N is measured at high pH, starting from the acid-unfolded ensemble, the formation of I_a occurs in the mixing time of the sub-millisecond stopped-flow, but the subsequent steps, the I_a ⇌ I_b and I_b ⇌ N reactions, exhibit similar kinetics by far-UV CD and Trp fluorescence, indicating that these two late stages of the apoMb folding process also occur in highly cooperative, two-state reactions.

Many small globular proteins fold by forming partly structured intermediates in the earliest times of their folding process. The mechanisms by which these early intermediates fold from an unfolded ensemble remain poorly understood, essentially because these reactions are too fast to be seen even with the fastest mixers available. With some proteins, including apomyoglobin, similar partially folded forms are observed at equilibrium under partially destabilizing conditions. Equilibrium characterization of these stable intermediates is easier and directly informs on the properties and behaviors of the more relevant kinetic intermediates. However, equilibrium studies provide information neither about the mechanism of the reaction nor about the properties of the transition state. Gaining this information relies only on kinetic studies.

Apomyoglobin (apoMb)[11] is particularly interesting to investigate the role of folding intermediates and the mechanism of their formation because this protein populates equilibrium intermediates near pH 4.0 under low-salt conditions that resemble kinetic intermediates observed when the protein refolds to its native conformation at pH 6.0 (*2*−*4*). In native conditions, all available data indicate that the native form N appears with a rate constant of about 2.5 s^{-1} at 5°C (*2*, *3*), but at least two different intermediates have been identified that form on very different time scales along this process. A prominent folding intermediate, named here I_a, forms during the dead-time of the fastest continuous flow mixing devices (<200 μs) (*2*−*3*, *5*−*7*). I_a has molten globule structural features, and hydrogen/deuterium (H/D) exchange experiments revealed that it contains a structured core formed by the A, H, and G helices of Mb as well as by a part of the B helix (*3*). The central part is more loosely packed and contains fluctuating D and E helices (*8*). A second intermediate, named I_b, forms more slowly with a rate constant of 35 s^{-1} at 5°C. I_b was first identified by stopped-flow Trp fluorescence (*2*), but its occurrence was since confirmed by other probes (*5*−*7*). Both intermediates, I_a and I_b, coexist near pH 4.0, in a equilibrium that depends on pH, the presence or absence of denaturant, and the presence or absence of stabilizing anions (*2*). Detailed structural characterization of the equilibrium mixture of I_a and I_b by NMR spectroscopy and by H/D exchange experiments reveals a similar structural organization to that of the dead-time intermediate at pH 6, with a stable and compact A(B)GH core and a central part containing fluctuating native and nonnative helices (*4*, *9*−*10*).

Although at pH 6 the formation of I_a is too fast to be seen, it was shown recently that folding and unfolding kinetics of

[†] This work was supported by the Emergence program (Région Rhône-Alpes, France).

* To whom correspondence should be addressed: Laboratoire de Biophysique Moléculaire et Cellulaire, Université Joseph Fourier, BMC/DRDC, 17 rue des Martyrs, 38054 Grenoble Cedex 9, France. Telephone: +(32) 4 38 78 42 12. Fax: + 32 4 38 78 54 87. E-mail: Marc.Jamin@cea.fr.

[1] Abbreviations: apoMb, apomyoglobin; Mb, myoglobin; CD, circular dichroism; N, native form; I, intermediate form; U, unfolded form; NATA, *N*-acetyl-tryptophanamide; NBS, *N*-bromosuccinimide; Trp, tryptophan.

10.1021/bi047372v CCC: $30.25
Published on Web 04/13/2005

I_a can be measured by stopped-flow Trp fluorescence within its urea-induced unfolding transition at pH 4.2 (*1*, *11*). When monitored by Trp fluorescence, refolding and unfolding kinetics of the U ⇌ I_a reaction follow exponential time courses of increasing and decreasing fluorescence intensity, respectively, in agreement with equilibrium fluorescence values (*1*). Unfolding kinetics at pH 4.2, however, deviates from a two-state model because of the presence of I_b and of aggregated forms of I. At pH 4.2, I_b is less stable than I_a and converts into I_a in the presence of moderate concentrations of urea (*2*). The unfolding transition observed above 1 M urea is that of I_a, but unfolding of I_b in this urea range gives rise to a burst phase in the unfolding kinetics (*1*, *11*). A second source of deviation from a strict two-state model comes from the presence of multimeric species that give rise to a second slow decreasing phase in unfolding kinetics (*1*, *11*). Besides these complications, the data are in agreement with predictions for a cooperative two-state U ⇌ I_a reaction (*12*, *13*). Plotting the apparent rate constant for folding and the fast apparent rate constant for unfolding as a function of urea concentration yields a V-shaped graph, typical of a two-state kinetic process. More importantly, the ΔG_{H_2O} and m values derived from these kinetic data are similar to those obtained from the analysis of the U ⇌ I_a equilibrium transition (*1*, *11*).

Additional evidence confirming that the U ⇌ I_a reaction is highly cooperative would be to compare the kinetics monitored by Trp fluorescence and by far-UV circular dichroism (CD) and find out whether secondary structure formation is concomitant with hydrophobic core formation and chain collapse. To perform this test, we use here a newly designed stopped-flow mixer and microcuvette assembly that operates with a dead-time of about 400 μs and monitor the folding and unfolding kinetics of I_a at pH 4.2 both by Trp fluorescence and by far-UV CD at 225 nm. We also extend the test to the other steps of the formation of native apoMb and measure refolding kinetics of N under native conditions by far-UV CD and Trp fluorescence.

MATERIALS AND METHODS

Urea, glucuronolactone, *N*-acetyl-tryptophanamide, *N*-bromo-succinimide, and lysozyme were purchased from Sigma. Concentration of urea solutions was determined from refractive index measurements (*14*). All experiments were performed in 2 mM citrate buffer containing 30 mM NaCl.

Protein Expression and Purification. Horse myoglobin was purchased from Sigma and apoMb was prepared by acid−acetone precipitation (*15*). Sperm whale apoMb was produced by heterologous expression in *Escherichia coli*. The synthetic gene for sperm whale myoglobin (*16*) was cloned between NdeI and BamHI sites in a pET17b expression vector (Novagen) of *E. coli*. The sequence of the cloned gene was verified by DNA sequencing. Protein was expressed in *E. coli* strain BL21 pLysS and purified according to the procedure described in ref *17*. Briefly, freshly transformed *E. coli* cells were grown in LB medium. Production was induced by addition of 1 mM IPTG when the O.D. at 600 nm reached 0.8. Cells were harvested 4 h after induction and were suspended in a lysis buffer (50 mM Tris buffer, 100 mM NaCl, 10 mM EDTA, pH 8.0). Crude extract was prepared by adding lysozyme and DNase. ApoMb was solubilized from the pellet by iterative extractions with a 0.1% trifluoroacetic solution. Fractions containing apoMb were identified by SDS PAGE and loaded on a radial-compression reversed-phase HPLC column (Delta-Pak C4, 15 μm, Waters) equilibrated in 0.1% TFA−25% acetonitrile and operating at 12 mL/min. The protein was eluted by a 25−60% acetonitrile linear gradient over 30 min. Collected fractions containing apoMb were pooled and lyophilized.

Protein solutions were prepared in distilled water, filtered, and dialyzed extensively against distilled water before use. Protein concentration was determined by absorbance in 6.0 M GdmCl (20 mM Na phosphate, pH 6.5) as described (*18*), using $\epsilon_{280\ nm} = 15\ 200\ M^{-1}\ cm^{-1}$ and $\epsilon_{288\ nm} = 10\ 800\ M^{-1}\ cm^{-1}$.

Circular Dichroism Spectroscopy. Equilibrium folding and unfolding CD experiments were performed with a Jasco J810 spectropolarimeter using a thermostated 1 cm quartz cell.

Stopped-Flow Measurements. Stopped-flow measurements were made by using a SFM-4 stopped-flow instrument (Bio-Logic, Claix, France). Kinetics were monitored simultaneously by Trp fluorescence and by far-UV CD with the same apparatus and the same observation chamber and settings. When both traces were measured simultaneously, a single wavelength, set at 225 nm, was used for both measuring the CD signal and for exciting Trp fluorescence. Fluorescence emission was detected at 90°, using an optical cutoff filter (50% transmittance at 305 nm). An excitation of Trp fluorescence at 288 nm yielded similar kinetics. The path length of the observation chamber was 0.8 mm. For CD measurements, a quartz blade was used to allow for corrections of the signal due to constraints on the quartz walls of the observation cell. Control experiments were performed with glucuronolactone to calibrate the CD signal and with lysozyme. Refolding of lysozyme exhibited typical measurable biphasic kinetics with an overshoot of CD signal corresponding to the formation of an intermediate.

Mixing efficiency and dead-time were measured by using the bimolecular quenching of *N*-acetyl-tryptophanamide (NATA) fluorescence by *N*-bromo-succinamide (NBS) (*19*). The reaction was measured in 10 mM sodium phosphate pH 7 at 20 °C. Final NATA concentration was 5 μM, and the kinetics were measured for NBS concentrations ranging from 0 to 10 mM. Kinetic traces were fitted to a one-exponential equation with the software provided by Bio-Logic. The dead-time of the apparatus was determined from a plot of $\ln(\Delta F_{Tot}/\Delta F_{Obs})$ versus k according to eq 1 (*20*), where t_0 is the dead-time and k is the apparent rate constant:

$$\ln(\Delta F_{Tot}/\Delta F_{Obs}) = t_0 k \quad (1)$$

For stopped-flow CD experiments performed at pH values ranging from 6.0 to 11.0, the unfolded protein at pH 2.2 was diluted in a 1:10 ratio into the refolding buffer. Final protein concentration was 10 μM, and the kinetic traces show averages of 15 individual measurements.

The refolding kinetics for the U ⇌ I_a reaction of sperm whale apoMb were measured at increasing temperature and analyzed with a one-exponential equation. The temperature dependence of the apparent rate constant ($1/\tau$) was modeled with the Arrhenius equation:

$$\ln\left(\frac{1}{\tau}\right) = \ln A - \frac{E_a}{RT} \quad (2)$$

where A is the preexponential factor, E_a is the activation energy, R is the gas constant, and T is the absolute temperature.

Fit to a Two-State Model. Folding and unfolding of I_a can be schematized with a two-state model:

$$U \underset{k_{21}}{\overset{k_{12}}{\rightleftharpoons}} I_a \quad (3)$$

for which the equilibrium constant is given by

$$K = \frac{[U]}{[I_a]} = \frac{k_{21}}{k_{12}} \quad (4)$$

and the apparent rate constant is given by

$$\frac{1}{\tau} = k_{12} + k_{21} \quad (5)$$

The equilibrium constant and the rate constants for folding (k_{12}) and unfolding (k_{21}) are expressed as functions of urea molarity ([urea]) using the standard relations (*12*−*13*):

$$K = K(H_2O)e^{(m[\text{urea}]/RT)} \quad (6a)$$

$$k_{12} = k_{12}(H_2O)e^{(m_{12}^{\neq}[\text{urea}]/RT)} \quad (6b)$$

$$k_{21} = k_{21}(H_2O)e^{(m_{21}^{\neq}[\text{urea}]/RT)} \quad (6c)$$

$K(H_2O)$, $k_{12}(H_2O)$, and $k_{21}(H_2O)$ represent the equilibrium constant and the rate constants for folding and unfolding at 0 M urea, respectively. The equilibrium parameters $\Delta G°$-$(H_2O)$and m, are related to the kinetics parameters $k_{12}(H_2O)$, $k_{21}(H_2O)$, $m_{12}^{\neq}$ and $m_{21}^{\neq}$ according to the following relations:

$$\Delta G°(H_2O) = -RT \ln \frac{k_{21}(H_2O)}{k_{12}(H_2O)} \quad (7a)$$

$$m = m_{21}^{\neq} - m_{12}^{\neq} \quad (7b)$$

From those equations, eq 8 can be derived according to the procedure described in ref *21* to represent the equilibrium urea-induced unfolding transition monitored by CD:

$$CD = \left[(CD_{Ia} + b_{Ia}[\text{urea}]) + (CD_U + b_U[\text{urea}]) \exp\left(-\frac{\Delta G°(H_2O)}{RT} + \frac{m[\text{urea}]}{RT}\right)\right] \Big/ \left[1 + \exp\left(-\frac{\Delta G°(H_2O)}{RT} + \frac{m[\text{urea}]}{RT}\right)\right] \quad (8)$$

where CD_U and CD_{Ia} are the CD values at 222 nm of U and I_a at 0 M urea, and b_U and b_{Ia} are the slopes of the linear baselines for the variation of the CD signal of U and I_a with urea concentration, respectively. Equation 9 can be derived to represent the dependence of the apparent rate constant $1/\tau$ versus urea molarity:

$$\frac{1}{\tau} = k_{12}(H_2O) \exp\left(\frac{m_{12}^{\neq}[\text{urea}]}{RT}\right) + k_{21}(H_2O) \exp\left(\frac{m_{21}^{\neq}[\text{urea}]}{RT}\right) \quad (9)$$

The kinetic parameters were determined in a combined fit of these two data sets (Figures 3 and 4) using SIGMAPLOT (Jandel, San Rafael, CA).

Modeling the pH Dependence of the Rate Constants. The rate constants for folding (k_{12}) and unfolding (k_{21}) are expressed as functions of pH by assuming that the proton binding sites are equivalent and independent, using the following equations:

$$k_{12} = k_{12}^{\text{ref}} \frac{\prod_i [1 + 10^{(pK_{ai}^{\neq} - pH)}]}{\prod_i [1 + 10^{(pK_{ai}^{U} - pH)}]} \quad (10a)$$

$$k_{21} = k_{21}^{\text{ref}} \frac{\prod_j [1 + 10^{(pK_{aj}^{\neq} - pH)}]}{\prod_j [1 + 10^{(pK_{aj}^{Ia} - pH)}]} \quad (10b)$$

$$K = \frac{k_{21}^{\text{ref}}}{k_{12}^{\text{ref}}} \quad (10c)$$

where k_{12}^{ref} and k_{21}^{ref} are the reference rate constants for the U → I_a and I_a → U reactions at high pH, respectively, K is the folding equilibrium constant at high pH, and the pK_{ai} and pK_{aj} values refer to residues i and j in the U, I_a, and $I^{\neq}$ forms. Simulations were performed with SIGMAPLOT (Jandel, San Rafael, CA).

RESULTS

A Sub-Millisecond Stopped-Flow Apparatus. Conventional stopped-flow instruments have dead-times on the order of 1 ms in the fluorescence detection mode and on the order of 5 ms in the CD (CD) mode. Here, we use a newly designed micromixer and microcuvette with reduced volumes (Bio-Logic, Claix, France) that operates with a similar dead-time in both fluorescence and CD modes. In the fluorescence mode, optimal settings of the instrument bring the dead-time down to 250 μs. These performances were obtained by reducing the mixer and cuvette volumes while keeping the solution flow rate as fast as possible. The cuvette has a light path of 0.8 mm and a volume of 4 μL. The maximum flow rate attainable with the SFM-400 system is 18−20 mL s^{-1}. However, transient mechanical stress due to pressure changes on the cuvette quartz wall produces a dynamic linear dichroism artifact that prevents measurements in CD mode at such high flow rate values. By using glucuronolactone and measuring the CD signal at 225 nm, we found that a maximum flow rate of 10−12 mL s^{-1} is usable in CD experiments. Static linear dichroism was also observed that originates from the vertical strain exerted by the cuvette mount. This linear dichroism signal was compensated by inserting a quartz blade before the observation cuvette that was set under an adjustable static strain oriented at a right angle from that exerted by the flow. The strain on the blade

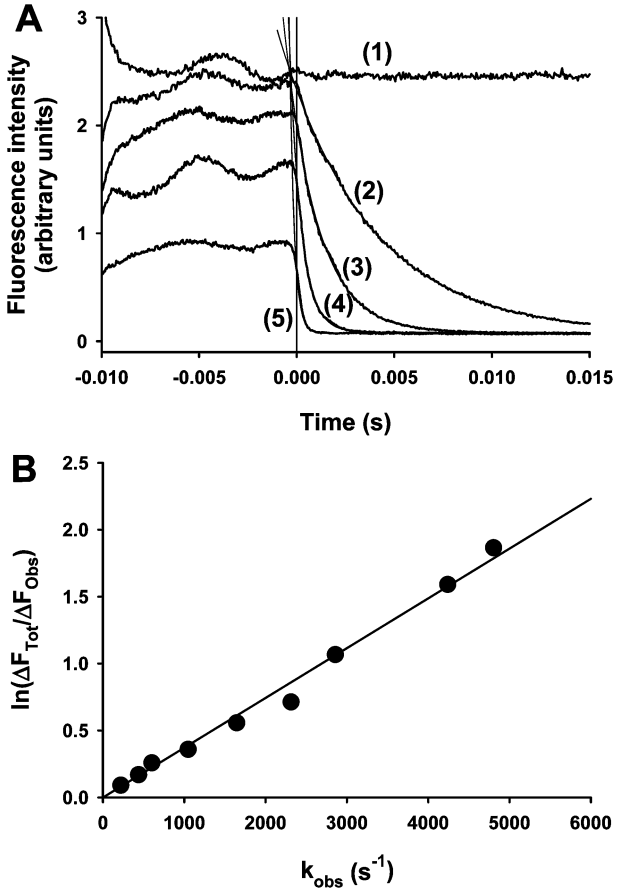

FIGURE 1: Tests of the sub-millisecond stopped-flow. (A) Bimolecular test reaction. Kinetics of the reaction between NATA at a final concentration of 5 μM and NBS at varying concentrations: 0 mM (curve 1), 0.3 mM (curve 2), 0.9 mM (curve 3), 2.4 mM (curve 4), and 6.0 mM (curve 5). Conditions: NATA and NBS are mixed in a 1:1 ratio in 10 mM phosphate buffer pH 7, 20 °C. The excitation was at 295 nm, and a cutoff filter at 320 nm was used for the emission. Curves 2 and 3 are fitted to a one-exponential equation. (B) Plot of $\ln(\Delta F_{tot}/\Delta F_{obs})$ versus k. ΔF_{tot} is the difference at time 0 between curve 1 and the final fluorescence measured. The slope of this graph provides a dead-time value of 370 ± 15 μs.

was adjusted by measuring the static CD value of a calibrated solution of glucuronolactone at 225 nm.

The efficiency of mixing and the dead-time of the apparatus in the settings used in CD mode are estimated by using a fluorescence quenching reaction between NATA and NBS (*14*). Mixing efficiency is estimated by monitoring fluorescence intensity when the liquid flows through the observation cell before the stop (Figure 1A). In our experiment, the optical signal was recorded during the flow for 10 ms before the stop, and time zero refers to the time at which liquid flow stops. Accordingly, the flowing period preceding the stop appears as negative time. Figure 1A shows that, during this time, fluorescence emission increases and reaches a plateau about 5 ms before the stop, indicating that mixing is complete. The kinetic traces from time zero are well fitted by a single-exponential equation and extrapolate to the initial fluorescence about 400 μs before time 0. A plot of the observed rate constant as a function of NBS concentration is linear, and its slope yields a value of 670 000 ± 11 000 M^{-1} s^{-1} for the second-order rate constant of the reaction. The dead-time is determined from a plot of $\ln(\Delta F_{Tot}/\Delta F_{Obs})$ versus k (Figure 1B), where ΔF_{Tot}, the total fluorescence change, is calculated for each curve as the difference between the fluorescence intensity of NATA and the fluorescence intensity at the end of the kinetics, and ΔF_{Obs} is the fluorescence amplitude of each kinetic curve measured from time 0 (*20*). The plot is linear, and its slope directly yields a dead-time of 370 ± 15 μs for the mixer. This dead-time is similar to that calculated by dividing the volume that separates the mixing chamber from the observation chamber by the flow rate. Whereas in these conditions this mixer only provides a two-fold improvement of the dead-time in fluorescence mode, as compared with classical mixer and cuvette, it provides a 10-fold improvement in CD mode since CD kinetics can be measured with the same mixing chamber and settings and thus with the same dead-time.

Folding and Unfolding Kinetics of I_a at pH 4.2. The refolding and unfolding kinetics of apoMb I_a are measured here within its urea-induced unfolding transition (above 1 M urea) both by Trp fluorescence and by far-UV CD at 225 nm. In the native protein, Trp fluorescence is usually considered as a probe of tertiary structure, but strictly it reports on the burial of Trp residues in a nonpolar environment. Upon formation of a folding intermediate from an unfolded ensemble, Trp fluorescence more likely reports on partial or global collapse of the polypeptide chain, leading to the burial of Trp side chains inside a hydrophobic core. Both horse and sperm whale apoMb have two Trp residues located in A helix, and both Trp residues become buried, at least partially, in the A(B)GH core in the folding intermediate. The changes in Trp fluorescence upon formation of I_a are thus used here as a probe of the collapse of this core, whereas changes in far-UV CD are used as a probe of secondary structure formation.

Figure 2 shows typical folding and unfolding kinetics for horse and sperm whale apomyoglobin. At equilibrium, I_a has a higher fluorescence intensity and a lower ellipticity at 225 than U. Accordingly, in refolding kinetics, fluorescence intensity increases and molar ellipticity at 225 nm decreases in single-exponential time courses (Figure 2A,B). No significant change occurs during the mixing time, and up to 90% of the reaction is observed. At the same final urea concentration, similar values of the observed rate constant are found for kinetics monitored either by Trp fluorescence or by far-UV CD. In unfolding kinetics, fluorescence intensity decreases and molar ellipticity at 225 nm increases (Figure 2C−F). The same complications are observed here as previously (*1*, *11*). The burst phase in Trp fluorescence, assigned to the conversion of I_b into I_a, is clearly visible in Figure 2C,E. By far-UV CD, the signal-to-noise ratio is too small to reveal the presence of a corresponding burst phase (Figure 2D,F). If, however, it occurs during the mixing time, the $I_b \rightleftharpoons I_a$ reaction involves only a small variation in CD signal, in agreement with other observations (*5*). With both probes two kinetic phases are measurable. The fast phase observed by Trp fluorescence was previously assigned to the $U \rightleftharpoons I_a$ reaction, and the slow phase, which is detected as a baseline change on the time scale shown in Figure 2, was assigned to the presence of aggregated species in the initial conditions (*1*). For the fast measurable phase, similar rate constants are obtained with both probes.

At pH 4.2, horse apoMb is less stable than sperm whale apoMb, and it unfolds at lower urea concentrations as shown when equilibrium urea-induced unfolding transitions are monitored by far-UV CD (Figure 3 and Table 1). As

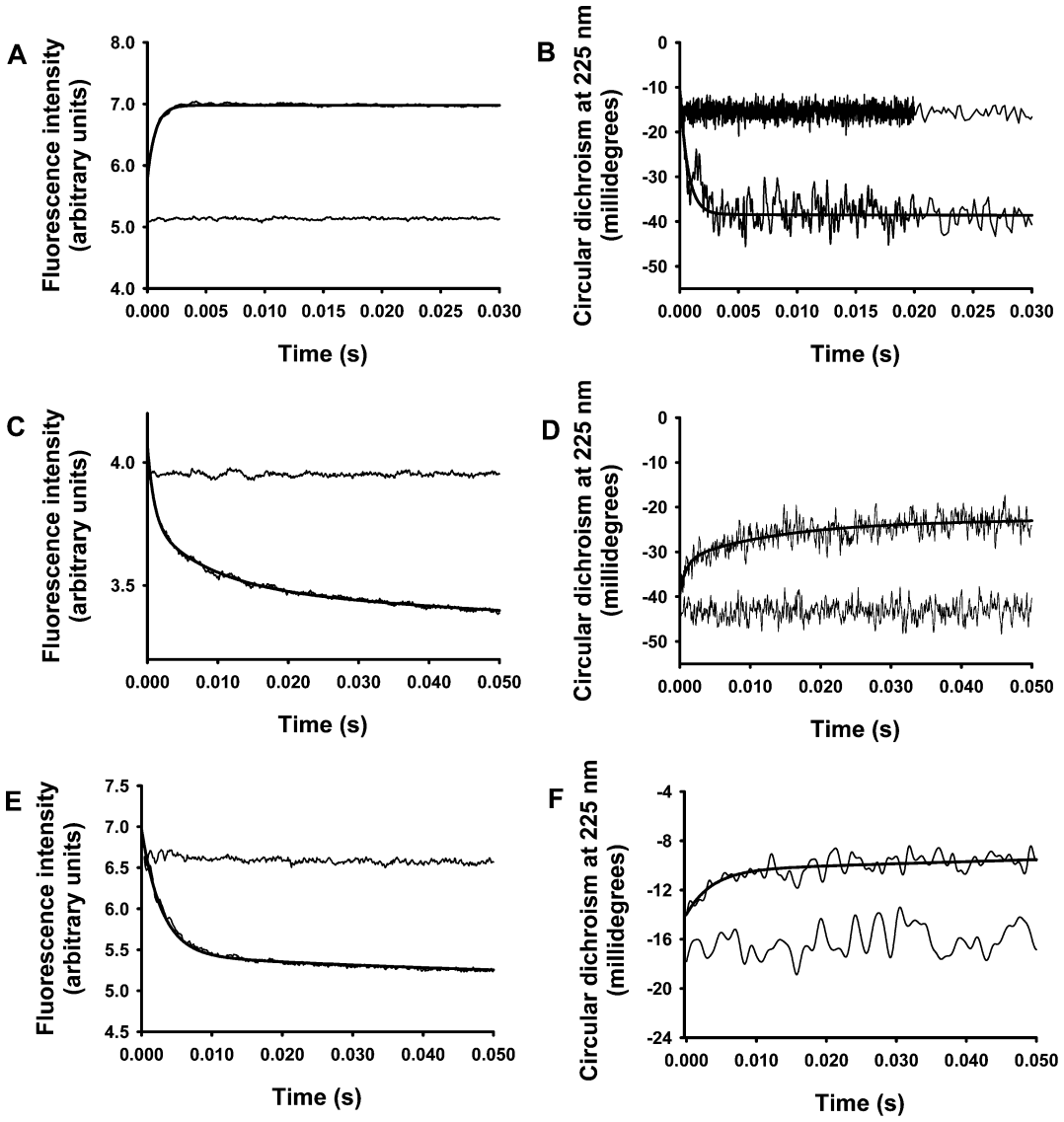

FIGURE 2: Urea-induced refolding (A, B) and unfolding (C−F) kinetics of the pH 4 intermediate measured by Trp fluorescence (A, C, E) and by far-UV CD (B, D, F) for horse (A−D) and sperm whale (E−F) apomyoglobin. The starting material for refolding experiments is U at pH 4.2 in 4 M urea and for unfolding it is a mixture of I_a and I_b at pH 4.2 in 0 M urea. The final urea concentration is 1.1 M (A, B) or 1.9 M urea (C−F). Stopped-flow fluorescence was monitored with an excitation at 225 nm and a cutoff filter at 305 nm for the emission. Stopped-flow CD was monitored at 225 nm. Fluorescence kinetics show averages of three shots, whereas CD kinetics show averages of about 20 shots. Kinetics are fitted to a one-exponential equation for refolding and to a two-exponential equation for unfolding. Conditions: 2 mM Na citrate, 30 mM NaCl, pH 4.2, 5 °C; final protein concentration is 50 μM (A, B), 100 μM (C, D), or 24 μM (E, F).

previously observed (*1*), final values in the kinetic experiments monitored by Trp fluorescence and far-UV CD reproduce the equilibrium unfolding transitions (data not shown). For both horse (Figure 4A) and sperm whale (Figure 4B) apoMb, a single V-shaped dependence is observed when the apparent rate constant for the U ⇌ I_a reaction is plotted as a function of urea concentration. For sperm whale apoMb (Figure 4B), the data obtained in this study are in agreement with previous kinetic data obtained by measuring Trp fluorescence with a stopped-flow apparatus operating with a dead-time of 1 ms (small circles in Figure 4B show data taken from ref *1*). Both equilibrium and kinetic data are modeled by assuming a two-state reaction (see Materials and Methods). The rate constants for folding (k_{12}) and unfolding (k_{21}) and their dependences on urea concentration ($m_{12}^{\neq}$ and $m_{21}^{\neq}$ values) have been obtained in a combined fitting procedure of the equilibrium constant (K) and of the apparent rate constant ($1/\tau$) (Table 1). According to a two-state model, the midpoint of the equilibrium transition occurs at the urea concentration (C_m) given by the following equation:

$$C_m = -RT\frac{\ln\left(\frac{k_{21}(H_2O)}{k_{12}(H_2O)}\right)}{m_{21}^{\neq} - m_{12}^{\neq}} \qquad (11)$$

whereas the lowest value of $1/\tau$ is found at a urea concentration ($C_{(1/\tau)min}$), where the first-order derivative with respect to urea concentration of the equation giving the urea-dependence of the apparent rate constant (eq 9 in Materials and Methods) is equal to zero:

$$C_{(1/\tau)min} = -RT\frac{\ln\left(-\frac{k_{21}(H_2O)m_{21}^{\neq}}{k_{12}(H_2O)m_{12}^{\neq}}\right)}{m_{21}^{\neq} - m_{12}^{\neq}} \qquad (2)$$

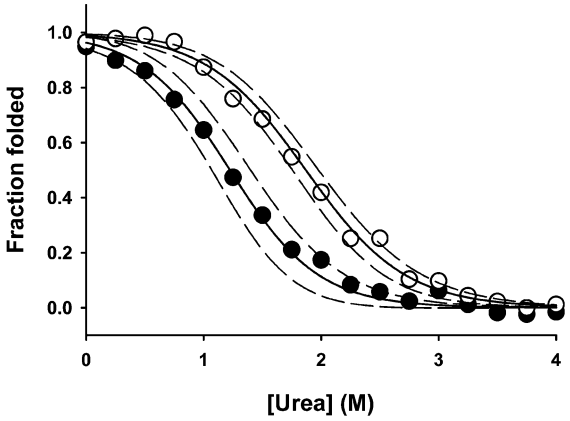

FIGURE 3: Equilibrium urea-induced unfolding transition for horse (●) and sperm whale (○). Urea-induced unfolding transitions were monitored by far-UV CD at 222 nm. The full lines are drawn using eq 8, and the parameters shown in Table 1. The dashed lines show the 95% confidence intervals for the combined fit of equilibrium and kinetic data. Conditions: 2 mM Na citrate, 30 mM NaCl, pH 4.2, 5 °C; final protein concentration is between 1 and 5 μM.

Table 1: Parameters of the Urea-Induced Unfolding Transition at pH 4.2

parameters	sperm whale	horse
$k_{12(H_2O)}$ (s^{-1})	3980 ± 800	6000 ± 1,500
$k_{21(H_2O)}$ (s^{-1})	47 ± 8	230 ± 50
m_{12} (cal/mol/M)	−900 ± 75	−1050 ± 150
m_{21} (cal/mol/M)	410 ± 30	420 ± 60
$C_{(1/\tau)min}$ (M)	2.2 ± 0.2	1.6 ± 0.2
$\Delta G_{(H_2O)}$ (cal/mol)	2450 ± 140	1800 ± 200
m (cal/mol/M)	1310 ± 80	1470 ± 160
C_m (M)	1.9 ± 0.2	1.2 ± 0.2

If the absolute value of $m_{12}^{\neq}$ is different from that of $m_{21}^{\neq}$, the value of C_m is close to that of $C_{(1/\tau)min}$ but not equal. According to the difference in equilibrium stability between the two proteins, the midpoint of the V-shaped plot ($C_{(1/\tau)min}$) is found at a lower urea concentration for horse apoMb than for sperm whale apoMb, but because the value of $m_{12}^{\neq}$ is larger than that of $m_{21}^{\neq}$, $C_{(1/\tau)min}$ values are larger than C_m values (Table 1). The lower stability of horse apoMb is mainly due to an increase of the unfolding rate.

Protein Concentration Dependence of the Folding Kinetics of I_a. Refolding kinetics for sperm whale apoMb at pH 4.2 were measured by stopped-flow Trp fluorescence at varying final protein concentrations, ranging from 1 to 8.8 μM. A solution of unfolded apoMb in 4 M urea was diluted 3 times in a refolding buffer at a final urea concentration of 1.9 M. Each kinetic curve could be fitted to a one-exponential equation. The amplitude of the kinetic curves exhibits a linear dependence on protein concentration (Figure 5A). The rate constant is similar for each protein concentration (Figure 5B) and matches that measured, at the same final urea concentration, at higher protein concentrations (Figure 2), showing that, in these conditions, the folding kinetics of the pH 4 intermediate of apoMb are not complicated by an aggregation process.

Temperature Dependence of the Folding Kinetics of I_a. Refolding kinetics for sperm whale apoMb at pH 4.2 were measured by stopped-flow Trp fluorescence at two different final urea concentrations and at various temperatures, ranging from 5 to 15 °C. Folding kinetics at the same final urea concentrations had been obtained previously at 20 °C by continuous-flow Trp fluorescence (*11*). Figure 6 shows the Arrhenius plots of these rate constants. Activation energies of 23.6 ± 0.4 and 22.3 ± 1.3 kcal/mol are obtained at final urea concentrations of 1.5 and 1.8 M, respectively, indicating that the U ⇌ I_a reaction involves a high energy barrier.

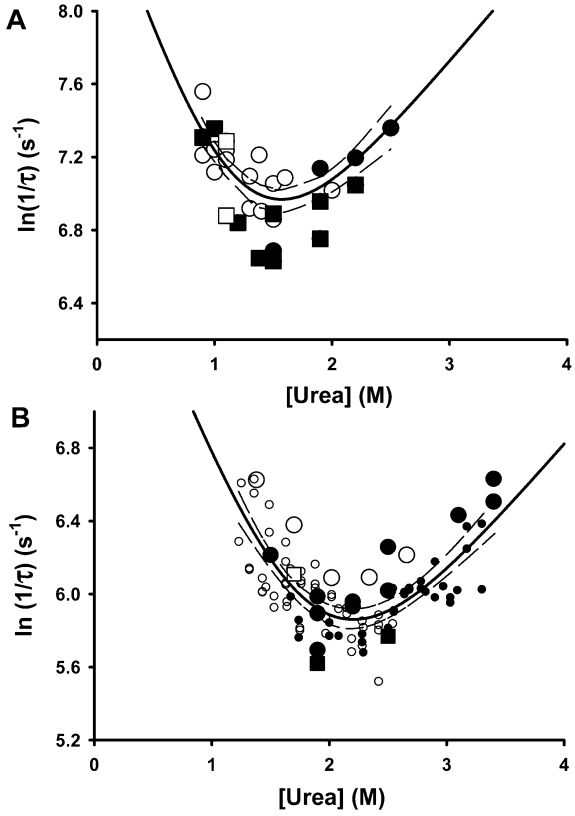

FIGURE 4: Apparent rate constants ($1/\tau$) versus [urea] for refolding from 4 M urea and for unfolding from 0 M urea. (A) Horse apomyoglobin. (B) Sperm whale apomyoglobin. Open symbols are for refolding kinetics, and closed symbols are for unfolding kinetics. Circles are for kinetics measured by Trp fluorescence, and squares are for kinetics measured by far-UV CD. Small open and closed circles in panel B show data taken from ref *1* that were measured by stopped-flow fluorescence in identical conditions. The full lines are drawn using eq 9 and the parameters shown in Table 1, and the dashed lines show the 95% confidence interval for the combined fit of equilibrium and kinetic data.

pH Dependence of the Folding Kinetics of I_a. A kinetic phase observed by monitoring Trp fluorescence in pH-jump experiments, starting from U at pH 2.0 and ending at final pH values below 3.5, has been previously assigned to the U ⇌ I_a reaction (*11*). The rate constant of this kinetic phase increases with pH and becomes too fast to be measured above pH 3.5. At pH 4.2, an estimate of the rate for the U ⇌ I_a reaction has been obtained by extrapolating to zero urea concentration, the rate constants measured within the urea-induced unfolding transition (*1*).

A simple model can be used to predict the pH dependence of the apparent rate constant for the U ⇌ I_a reaction. This model is adapted from the Monod-Wyman-Changeux model (MWC model) (*22*) to describe the effect of preferential binding of *n* protons on folding and unfolding kinetics. This model has been applied previously to simulate the pH dependence of kinetics for the I ⇌ N reaction of apomyoglobin at higher pH values (*23*). For kinetics induced by pH change, the preferential binding of protons results in lowered pK_a values of the contributing residues in both I_a and in the

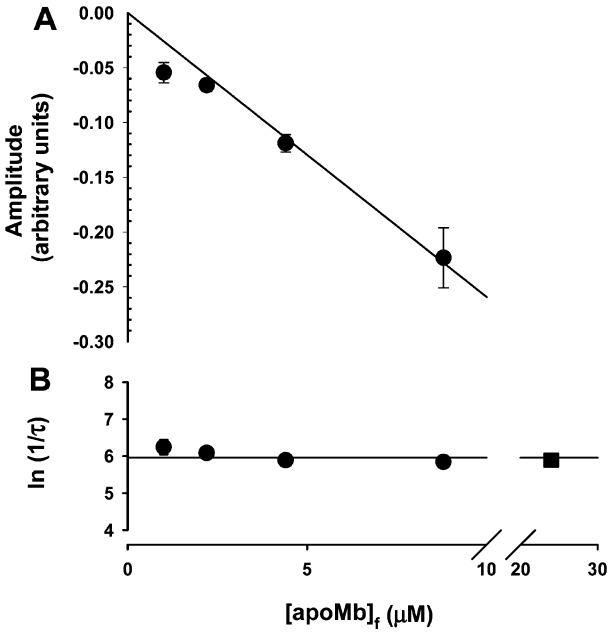

FIGURE 5: Protein concentration dependence of the folding kinetics of I_a. Refolding kinetics were measured by Trp fluorescence following a urea-jump from 4 M urea to 1.9 M urea. The kinetics were fitted with a one-exponential equation. Error bars represent the standard deviation. (A) Plot of the amplitude versus final protein concentration. (B) Plot of the apparent rate constant versus final protein concentration. The filled square shows the observed rate at 1.9 M urea obtained by measuring Trp fluorescence in the conditions used in Figure 2 (excitation wavelength = 225 nm). Conditions: 2 mM Na citrate, 30 mM NaCl, pH 4.2, 5 °C; mixing ratio 1:3; excitation wavelength was set at 288 nm.

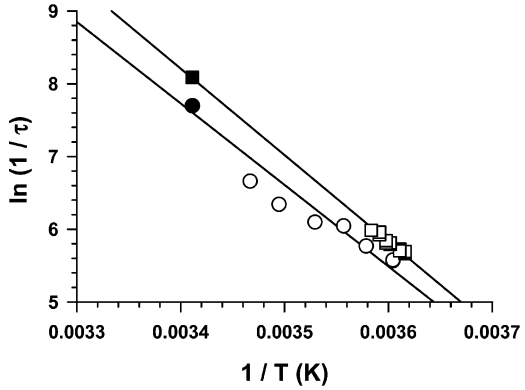

FIGURE 6: Arrhenius plots for the apparent rate constant of the U ⇌ I_a reaction for sperm whale apoMb. Refolding kinetics were measured at two different final urea concentrations and at different temperatures by stopped-flow fluorescence: (○) [urea] = 1.5 M, (□) [urea] = 1.8 M. Kinetics were fitted to a one-exponential equation, and the plot shows the logarithm of the apparent rate constant ($1/\tau$) as a function $1/T$. The closed symbols shows the apparent rate constant for unfolding obtained at 20 °C at the same final urea concentrations, using a continuous-flow fluorescence apparatus (data taken from ref *11*). The lines are drawn using eq 2.

transition of the U ⇌ I_a reaction. The model relies on the assumptions that all groups responsible for the transition are equivalent and independent and thus do not vary with titration of other ionizable groups.

The A(B)GH core of apoMb contains 13 acidic groups. If we assume that these groups have model compound pK_a in U (a pK_a = 4.1 is taken as an average between Glu and Asp pK_a values), a lower pK_a in I_a (pK_a = 3.6) and an intermediate pK_a in the transition state, closer to that of I_a than to that of

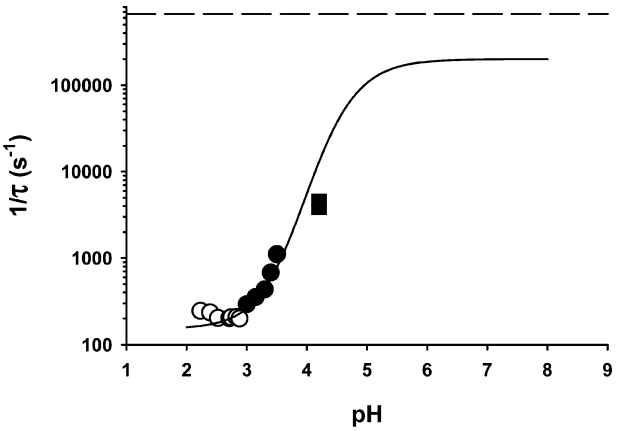

FIGURE 7: pH dependence of the time constant for the U ⇌ I_a reaction. Folding and unfolding kinetics for sperm whale apoMb at 4.5 °C were induced by pH-jump, starting from pH 2.2 for refolding or from pH 6.0 for unfolding. The symbols show the apparent rate constant for folding (●) and for unfolding (○). The filled squares (■) show the apparent rate for folding at pH 4.2 obtained by extrapolating data within the urea-induced unfolding transition for both sperm whale and horse apoMb. The line shows a prediction of the apparent rate constant for the U ⇌ I_a reaction, calculated using a simple model (eq. where acidic groups in the A(B)GH core have different pK_a values in U (pK_a = 4.1), I_a (pK_a = 3.6) and in the transition state separating U from I_a (pK_a = 3.8) and using k_{12}^{ref} = 200 000 s^{-1}, k_{21}^{ref} = 20 s^{-1}, i = 11 and j = 2. The dashed line shows the fastest rate predicted for collapse of apoMb (*53*).

U (pK_a = 3.8), then the model predicts a large increase of the apparent rate constant with pH in fair agreement with available data (Figure 7). Although the choice of pK_a values is arbitrary, this simulation provides a rationale for the variation of the rate constant with pH. It should be noted also that the Linderstrøm-Lang smeared charge model has also been used for simulating equilibrium acid-induced unfolding transition (*24*) and that similar pH dependences are obtained with this model.

Folding of N under Native Conditions. Refolding kinetics of N, starting from U at pH 2.2, were measured here at various final pH values ranging from pH 6.0 to pH 11.0, both by Trp fluorescence and by far-UV CD at 225 nm. In this pH range, kinetics monitored by Trp fluorescence are similar. They clearly show a burst phase followed three measurable exponential phases, corresponding to the previously assigned I_a ⇌ I_b, I_b ⇌ N, and I_{agg} ⇌ N reactions (*2*). The rate constants for each measurable phase do not change significantly (data not shown), but the ratio of the amplitude for the fast (I_a ⇌ I_b reaction) over that for the middle phase (I_b ⇌ N reaction) changes from 0.7 at pH 6.0 to 1.4 at pH 11.0, indicating that I_b is more populated at pH 11.0 than at pH 6.0.

By far-UV CD, a major kinetic phase is detected whose rate constant matches exactly that measured by Trp fluorescence for the I_b ⇌ N reaction. At pH 6.0, the I_a ⇌ I_b reaction is not clearly detectable by far-UV CD but, when refolding kinetics are monitored at pH 11.0, a fast phase corresponding to the I_a ⇌ I_b reaction seen by fluorescence is also apparent in the kinetics monitored by far-UV CD (Figure 8A). The kinetic trace by far-UV CD is better fitted with a two-exponential equation than with a one-exponential equation (Figure 8B−D), and the rate constants for the two phases match those measured by Trp fluorescence. These results

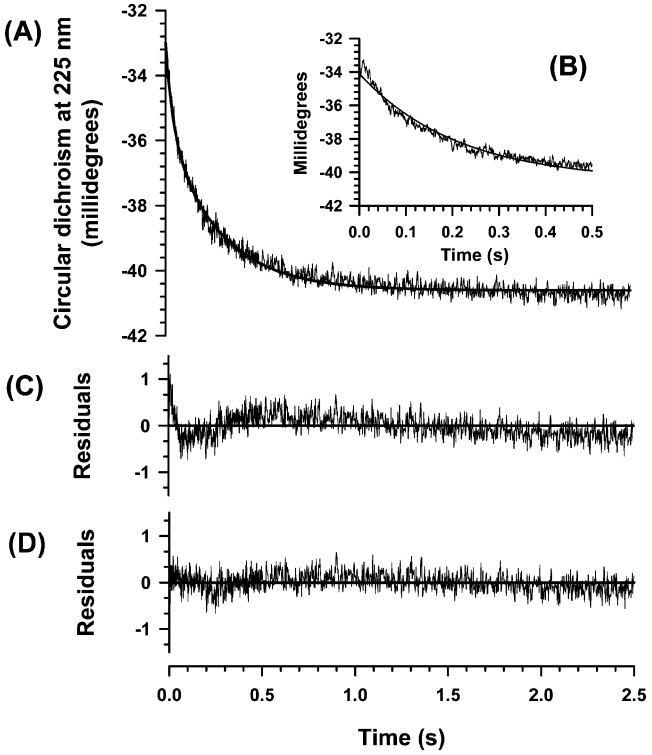

FIGURE 8: Refolding kinetics at pH 11 measured by far-UV CD. (A) Refolding kinetics following a pH jump from pH 2.2 to pH 11.0. The fit to a two-exponential equation is shown as a line and yields the following parameters: $A_1 = 2.60 \pm 0.06$ millidegrees, $A_2 = 5.05 \pm 0.03$ millidegrees, $k_1 = 25.0 \pm 1$ s^{-1}, $k_2 = 3.55 \pm 0.04$ s^{-1} and $CD_{final} = -40.60 \pm 0.03$ millidegrees. (B) The insert shows the same data fitted to a one-exponential equation. (C) Residuals for fitting to a one-exponential equation. (D) Residuals for fitting to a two-exponential equation. Conditions: 2 mM Na citrate, 30 mM NaCl, 5 °C; final protein concentration is 10 μM.

suggest that the $I_a \rightleftharpoons I_b$ reaction also gives rise to a change in CD signal, but one that is more difficult to detect because of the lower signal-to-noise ratio in CD than in the fluorescence signal. The slowest phase corresponding to the formation of N from an aggregated fraction of I is not resolved in the kinetics monitored by far-UV CD.

DISCUSSION

Folding Pathway of apoMb. The folding process of apoMb has been extensively characterized in both equilibrium and kinetic studies (*25*−*26*). Similar intermediates are found both as stable species at equilibrium near pH 4 and as transient species during refolding kinetics at pH 6 (*3*−*4*). Both forms are compact, with a radius of gyration of the order of 23 Å (*5*, *27*). They contain a hydrophobic core in which both Trp residues are buried, and they contain between 45 and 60% of the helical Mb structure (*3*−*5*), but they lack the tight packing of the side chains (*7*, *28*). However, both equilibrium and kinetic intermediates are heterogeneous in nature and consist of ensembles of conformations. In addition, two different intermediate forms, I_a and I_b, separated by a sizable kinetic barrier, have been identified by Trp fluorescence (*2*). The existence of a second intermediate was already suggested in the original pulse labeling H/D exchange experiments in which residues in the B helix were found to acquire protection against H/D exchange more slowly than those forming the AGH core but more rapidly than those forming the rest of the protein (*3*). These pulse labeling experiments were performed in the presence of 0.8 M urea, and I_b is sensitive to the presence of urea. In the presence of 0.8 M urea, the relative amplitude of the $I_a \rightleftharpoons I_b$ reaction in refolding kinetics monitored by Trp fluorescence at pH 6.0 is reduced as compared to that measured in the absence of denaturant (data not shown). More recent H/D exchange experiments confirm the heterogeneous nature of the burst phase intermediate by revealing the presence of labile secondary structures in B helix, at the junction between D and E helices, and inside E helix (*8*). The occurrence of the $I_a \rightleftharpoons I_b$ reaction in the refolding process of N has also been detected by different probes with both horse and sperm whale apoMb (*5*−*7*). A kinetic phase with a rate constant similar to that measured for the $I_a \rightleftharpoons I_b$ reaction by Trp fluorescence was measured when folding of native horse apoMb was monitored with a sub-millisecond continuous-flow apparatus by far-UV CD (*5*) and by resonance Raman spectroscopy (*6*) in pH-jump experiments, starting from U at pH 2. Here, we show that, with sperm whale apoMb, the $I_a \rightleftharpoons I_b$ reaction is not resolved by far-UV CD at pH 6.0 but is resolved at pH 11.0, certainly because I_b is more populated at pH 11.0 than at pH 6.0. In native conditions, the $I_a \rightleftharpoons I_b$ reaction was not detected in kinetics monitored by SAXS (*5*), but pulsed thiol-disulfide exchange experiments, carried out with sperm whale apoMb variants, indicate that side chain packing at the BG interface occurs on the same time scale (*7*). These data suggest that formation of I_b involves no major change in the compaction of the chain but rather corresponds to the strengthening of the helical structure already present in I_a and to the stabilization of the A(B)GH core. This hypothesis is supported by the observations that some of the marginally stable helices present in the intermediate are recruited in the structured core upon single mutation (*29*, *30*) or by addition of a stabilizing anion (*28*).

Two major arguments point toward a linear $U \rightleftharpoons I_a \rightleftharpoons I_b \rightleftharpoons N$ model where I_a and I_b are compulsory on-pathway intermediates. First, all observed intermediate forms of apoMb contain essentially nativelike structure (*3*−*10*) and can be arranged in a series where structure and compaction are progressively acquired (*17*). Second, two kinetic studies provide supporting evidence for the linear model and exclude simple models either where N is formed by parallel fast and slow pathways or where I is a dead-end complex (*2*, *31*).

ApoMb from two species are commonly used in folding studies, those from sperm whale and horse. They have usually been used in different conditions, and no formal comparison of their folding process has been done. Here, we found that both proteins exhibit similar folding kinetics at pH 4.2, even if faster unfolding is measured for horse apoMb than for sperm whale apoMb, suggesting that the folding intermediate is not as stable in horse as in sperm whale apoMb.

Cooperativity in apoMb Folding Process. Cooperativity in proteins arises because stabilizing interactions cooperate to stabilize the structure and provide an overall stabilizing effect larger than the sum of each individual contribution (*32*). Practically, a highly cooperative folding behavior means that no intermediate is detected during a folding/unfolding transition, and thus this transition can be described by a simple two-state model in which the initial and final states are separated by a unique free energy barrier. Native

conformations bear hallmarks of highly cooperative structures and are separated from the denatured ensemble by a large kinetic barrier. However, many proteins fold through folding intermediates, which are distinct from the unfolded ensemble and more strictly consist of ensembles of collapsed and fluctuating conformations. Whether the formation of these intermediates from the unfolded ensemble is highly cooperative or not is still extensively debated.

Different tests have been applied for determining whether the formation of apoMb pH 4 intermediate from the unfolded ensemble is highly cooperative. A major test for cooperativity is the calorimetric test: in a two-state process, the enthalpy change measured by calorimetry should be equivalent to the effective van't Hoff enthalpy change calculated from the equilibrium thermal unfolding transition (*12*, *33*). Although the apoMb pH 4 intermediate exhibits a broad but measurable thermal unfolding transition, no significant enthalpy change is detected either by differential scanning calorimetry (*34*) or by isothermal titration calorimetry at 20 °C upon acid unfolding (*35*). The failure of the calorimetric test can result from the presence of more than two species in the mixture (*36*), and, at pH 4.2, we found that apoMb exists in at least two different forms, I_a and I_b (see above). At pH 2.2, where apoMb forms a similar intermediate in the presence of anions, a small but measurable excess of heat is released upon thermal unfolding (*37*).

Conversely, several other tests, including the kinetic experiments described here, support a highly cooperative mechanism for the formation of I_a. First, urea-induced equilibrium unfolding transitions measured at pH 4.2 by far-UV CD and by Trp fluorescence can be superimposed (*1*, *38*). Second, the introduction by site-directed mutagenesis of a glycine or of a proline residue in the middle of A or G helix affects the overall stability and the structure of the intermediate (*39*), as expected for a highly cooperative system. Third, a kinetic test, that is more sensitive to the presence of intermediates than equilibrium measurements (*13*) has confirmed the two-state behavior of the U ⇌ Ia reaction above 1 M urea (*1*, *11*).

Data reported here show that the compaction of the A(B)-GH core and the formation of secondary structure occur concomitantly, in single-exponential kinetics with similar apparent rate constants. In its urea-unfolded form, apoMb is expanded and devoid of almost any secondary structure, and thus formation of I_a at pH 4.2 from the urea-unfolded ensemble requires the collapse of the polypeptide chain, the formation of α-helices, and the packing of these helices into the A(B)GH core. The large temperature dependence of the apparent rate for refolding of I_a supports the presence of a large free-energy barrier separating U and I_a and the two-state character of the reaction. If single-exponential kinetics can be observed with multiple-state systems (*40*, *41*), the existence of a large free-energy barrier and the observation of similar kinetics by far-UV CD and by Trp fluorescence are more difficult to explain with a gradual model than with a two-state model. It is not clear however whether the signal change in Trp fluorescence reports on the global collapse of the polypeptide chain into a compact hydrophobic core, or if it reports only on the compaction of a previously collapsed chain, restricting the accessibility of the hydrophobic interior to solvent molecules. Several studies show that a rapid collapse of the chain could precede the rate-limiting step leading to the formation of the first stable intermediate (*42*−*44*). On another hand, different results suggest that protein collapse can be highly cooperative, exhibiting features of a barrier-limited process, such as single-exponential kinetics and large Arrhenius temperature dependences (*45*). Using a laser T-jump apparatus, Hagen and Eaton monitored the collapse of cytochrome C and found that these kinetics display typical features of a two-state process (*45*). For this reaction, they measured activation energy of the order of 28 kJ mol^{-1}, the same order of magnitude as for the activation energy measured here for the formation of I_a. With lysozyme, a prominent folding intermediate is formed during the dead-time of stopped-flow mixers. Application of the superposition test to curves where burst phase changes measured by Trp fluorescence and by far-UV CD are plotted against final guanidinium chloride concentrations reveals that the collapse of lysozyme is also a cooperative process (*46*). With α-lactalbumin, formation of the A state appears noncooperative according to various relevant tests (*47*−*49*), but a variant, lacking all four disulfide bridges, exhibits a more cooperative behavior as judged by the superposition test of equilibrium unfolding curves (*50*, *51*). With apoMb, the cooperativity can also be modulated by mutations or by the addition of anions (*39*, *52*). Cooperativity has been linked to stability (*39*), and the formation of I_a could require a concerted process because a minimal stability must be reached to maintain the nascent structure.

It should also be noted that unfolding kinetics of a low pH form of apoMb, named E, also exhibits features of a cooperative two-state process since one of the two kinetics phases detected by infrared absorbance (IR) spectroscopy also gives rise to a change in Trp fluorescence (*53*, *54*). The second phase seen by IR spectroscopy is not detected by Trp fluorescence.

Why is the Formation of I_a So Slow near pH 4? Recent studies have been carried out to estimate the upper limit of folding rate. Although it is still debated which theory should be used to predict folding rates, it seems that a consensus between experiments and theoretical predictions for the maximum rate constant attainable for an overall collapse and folding reaction is given by $^1/_\tau = 10^8/N\ s^{-1}$, where N is the number of residues of the protein (*55*). This estimate would set a limit at 670 000 s^{-1} ($\tau = 1.5\ \mu s$) for apomyoglobin folding reaction. In our studies, the formation of the first stable intermediate, containing secondary structure and hydrophobic packing is too fast to be measured at pH 6.0 with our mixing apparatus but occurs much more slowly at lower pH values, with a rate constant of 4000 s^{-1} ($\tau = 250\ \mu s$) at pH 4.2 and a rate constant of 300 s^{-1} at pH 3.0 ($\tau = 3300\ \mu s$) (*11*).

Why would the rate decrease at lower pH? Decreasing the pH reduces the stability of the intermediate, very likely because of the build-up of a net positive charge on the protein (*24*). Because it is more favorable to have multiple positive charges on an expanded form of the protein (U) than on a compact one (I_a), electrostatic repulsions lead to the progressive destabilization of I_a when the pH is decreased. If the transition state for the U ⇌ I_a reaction has a compaction level close to that of I_a, it is likely that its stability is also reduced when the pH is decreased, and thus that the rate constant for folding decreases.

ACKNOWLEDGMENT

We thank Prof. Buzz Baldwin for critical reading of the manuscript.

REFERENCES

1. Jamin, M., and Baldwin, R. L. (1996) Refolding and unfolding kinetics of the equilibrium folding intermediate of apomyoglobin, *Nat. Struct. Biol. 3*, 613−618.
2. Jamin, M., and Baldwin, R. L. (1998) Two forms of the pH 4 folding intermediate of apomyoglobin, *J. Mol. Biol. 276*, 491−504.
3. Jennings, P. A., and Wright, P. E. (1993) Formation of a molten globule intermediate early in the kinetic folding pathway of apomyoglobin, *Science 262*, 892−896.
4. Hughson, F. M., Wright, P. E., and Baldwin, R. L. (1990) Structural characterization of a partly folded apomyoglobin intermediate, *Science 249*, 1544−1548.
5. Uzawa, T., Akiyama, S., Kimura, T., Takahashi, S., Ishimori, K., Morishima, I., and Fujisawa, T. (2004) Collapse and search dynamics of apomyoglobin folding revealed by submillisecond observations of alpha-helical content and compactness, *Proc. Natl. Acad. Sci. U.S.A. 101*, 1171−1176.
6. Haruta, N., and Kitagawa, T. (2002) Time-resolved UV resonance Raman investigation of protein folding using a rapid mixer: characterization of kinetic folding intermediates of apomyoglobin, *Biochemistry 41*, 6595−6604.
7. Ha, J. H., and Loh, S. N. (1998) Changes in side chain packing during apomyoglobin folding characterized by pulsed thiol-disulfide exchange, *Nat. Struct. Biol. 5*, 730−737.
8. Nishimura, C., Dyson, H. J., and Wright, P. E. (2002) The apomyoglobin folding pathway revisited: structural heterogeneity in the kinetic burst phase intermediate, *J. Mol. Biol. 322*, 483−489.
9. Eliezer, D., Yao, J., Dyson, H. J. and Wright, P. E. (1998) Structural and dynamic characterization of partially folded states of apomyoglobin and implications for protein folding, *Nat. Struct. Biol. 5*, 148−155.
10. Eliezer, D., Chung, J., Dyson, H. J., and Wright, P. E. (2000) Native and non-native secondary structure and dynamics in the pH 4 intermediate of apomyoglobin, *Biochemistry 39*, 2894−2901.
11. Jamin, M., Yeh, S. R., Rousseau, D. L., and Baldwin, R. L. (1999) Submillisecond unfolding kinetics of apomyoglobin and its pH 4 intermediate, *J. Mol. Biol. 292*, 731−740.
12. Tanford, C. (1970) Protein denaturation. Part C. Theoretical models for the mechanism of denaturation, *Adv. Prot. Chem. 24*, 2−95.
13. Jackson, S. E., and Fersht, A. R. (1991) Folding of chymotrypsin inhibitor 2. 1. Evidence for a two-state transition, *Biochemistry 30*, 10428−10435.
14. Pace, C. N., Shirley, B. A. and Thompson, J. A. (1989) Measuring the conformational stability of a protein, in *Protein Structure*: *A Practical Approach* (Creighton, T. E., Ed.) pp 311−330, IRL Press, Oxford, UK.
15. Fanelli, A. R., Antonini, E. and Caputo, A. (1958) Studies on the structure of hemoglobin. I. Physicochemical properties of human globin, *Biochim. Biophys. Acta 30*, 608−615.
16. Springer, B. A. and Sligar, S. G. (1987) High-level expression of sperm whale myoglobin in *Escherichia coli*, *Proc. Natl. Acad. Sci. U.S.A. 84*, 8961−8965.
17. Jennings, P. A., Stone, M. J., and Wright, P. E. (1995) Overexpression of myoglobin and assignment of its amide, C alpha and C beta resonances, *J. Biomol. NMR 6*, 271−276.
18. Edelhoch, H. (1967) Spectroscopic determination of tryptophan and tyrosine in proteins, *Biochemistry 6*, 1948−1954.
19. Peterman, B. F. (1979) Measurement of the dead time of a fluorescence stopped-flow instrument, *Anal. Biochem. 93*, 442−444.
20. Hiromi, K. (1979) *Kinetics of Fast Enzyme Reactions*: *Theory & Practice*, John Wiley & Sons, New York.
21. Santoro, M. M., and Bolen, D. W. (1988) Unfolding free energy changes determined by the linear extrapolation method. 1. Unfolding of phenylmethanesulfonyl alpha-chymotrypsin using different denaturants, *Biochemistry 27*, 8063−8068.
22. Monod, J., Wyman, J. and Changeux, J. P. (1965) On the nature of allosteric transitions: A plausible model, *J. Mol. Biol. 12*, 88−118.
23. Jamin, M., Geierstanger, B. and Baldwin, R. L. (2001) The pK_a of His24 in the folding transition state of apomyoglobin, *Proc. Natl. Acad. Sci. U.S.A. 98*, 6127−6131.
24. Kay, M. S., and Baldwin, R. L. (1998) Alternative models for describing the acid unfolding of the apomyoglobin folding intermediate, *Biochemistry 37*, 7859−7868.
25. Wright, P. E., and Baldwin, R. L. (2000) Case study 1: The folding process of apomyoglobin, in *Mechanisms of Protein Folding* (Pain, R. H., Ed.) pp 309−329, Oxford University Press, Oxford, UK.
26. Jamin, M. (2005) Apomyoglobin folding process, *Prot. Pept. Lett.*, in press.
27. Kataoka, M., Nishii, I., Fujisawa, T., Ueki, T., Tokunaga, F., and Goto, Y. (1995) Structural characterization of the molten globule and native states of apomyoglobin by solution X-ray scattering, *J. Mol. Biol. 249*, 215−228.
28. Loh, S. N., Kay, M. S., and Baldwin, R. L. (1995) Structure and stability of a second molten globule intermediate in the apomyoglobin folding pathway, *Proc. Natl. Acad. Sci. U.S.A. 92*, 5446−5450.
29. Garcia, C., Nishimura, C., Cavagnero, S., Dyson, H. J., and Wright, P. E. (2000) Changes in the apomyoglobin folding pathway caused by mutation of the distal histidine residue, *Biochemistry 39*, 11227−11237.
30. Kiefhaber, T., and Baldwin, R. L. (1995) Intrinsic stability of individual alpha helices modulates structure and stability of the apomyoglobin molten globule form, *J. Mol. Biol. 252*, 122−132.
31. Tsui, V., Garcia, C., Cavagnero, S., Siuzdak, G., Dyson, H. J., and Wright, P. E. (1999) Quench-flow experiments combined with mass spectrometry show apomyoglobin folds through and obligatory intermediate, *Protein Sci. 8*, 45−49.
32. Creighton, T. E. (1995) Protein folding. An unfolding story, *Curr. Biol. 5*, 353−356.
33. Privalov, P. L. (1979) Stability of proteins: small globular proteins, *Adv. Prot. Chem. 33*, 167−241.
34. Griko, Y. V., and Privalov, P. L. (1994) Thermodynamic puzzle of apomyoglobin unfolding, *J. Mol. Biol. 235*, 1318−1325.
35. Jamin, M., Antalik, M., Loh, S. N., Bolen, D. W., and Baldwin, R. L. (2000) The unfolding enthalpy of the pH 4 molten globule of apomyoglobin measured by isothermal titration calorimetry, *Protein. Sci. 9*, 1340−1346.
36. Freire, E. (1995) Thermodynamics of partly folded intermediates in proteins, *Annu. Rev. Biophys. Biomol. Struct. 24*, 141−165.
37. Nishii, I., Kataoka, M., Tokunaga, F., and Goto, Y. (1994) Cold denaturation of the molten globule states of apomyoglobin and a profile for protein folding, *Biochemistry 33*, 4903−4909.
38. Kay, M. S., and Baldwin, R. L. (1996) Packing interactions in the apomyglobin folding intermediate, *Nat. Struct. Biol. 3*, 439−445.
39. Luo, Y., Kay, M. S., and Baldwin, R. L. (1997) Cooperativity of folding of the apomyoglobin pH 4 intermediate studied by glycine and proline mutations, *Nat. Struct. Biol. 4*, 925−930.
40. Tsong, T. Y., and Baldwin, R. L. (1972) A sequential model of nucleation-dependent protein folding: kinetic studies of ribonuclease A, *J. Mol. Biol. 63*, 453−469.
41. Parker, M. J., and Marqusee, S. (2000) A statistical appraisal of native state hydrogen exchange data: evidence for a burst phase continuum?, *J. Mol. Biol. 300*, 1361−1375.
42. Agashe, V. R., Shastry, M. C. R., and Udgaonkar, J. B. (1995) Initial hydrophobic collapse in the folding of barstar, *Nature 377*, 754−757.
43. Sadqi, M., Lapidus, L. J., and Muñoz (2003) How fast is protein hydrophobic collapse? *Proc. Natl. Acad. Sci. U.S.A. 100*, 12117−12122.
44. Magg, C., and Schmid, F. X. (2004) Rapid collapse precedes the fast two-state folding of the cold shock protein, *J. Mol. Biol. 335*, 1309−1323.
45. Hagen, S. J., and Eaton, W. A. (2000) Two-state expansion and collapse of a polypeptide, *J. Mol. Biol. 301*, 1019−1027.
46. Bachmann, A., Segel, D., and Kiefhaber, T. (2002) Test for cooperativity in the early kinetic intermediate in lysozyme folding, *Biophys. Chem. 96*, 141−151.
47. Xie, D., Bhakuni, V., and Freire, E. (1991) Calorimetric determination of the energetics of the molten globule intermediate in protein folding: apo-alpha-lactalbumin, *Biochemistry 30*, 10673−10678.

48. Schulman, B. A., and Kim, P. S. (1996) Proline scanning mutagenesis of a molten globule reveals non-cooperative formation of a protein's overall topology, *Nat. Struct. Biol. 3*, 682−687.
49. Schulman, B. A., Kim, P. S., Dobson, C. M. and Redfield, C. (1997) A residue-specific NMR view of the non-cooperative unfolding of a molten globule, *Nat. Struct. Biol. 4*, 630−634.
50. Redfield, C., Schulman, B. A., Milhollen, M. A., Kim, P. S., & Dobson, C. M. (1999) α-lactalbumin forms a compact molten globule in the absence of disulfide bonds, *Nat. Struct. Biol. 6*, 948−952.
51. Luo, Y., & Baldwin, R. L. (1999) The 28−111 disulfide bond constrains the alpha-lactalbumin molten globule and weakens its cooperativity of folding, *Proc. Natl. Acad. Sci. U.S.A. 96*, 11283−11287.
52. Kay, M. S., Ramos, C. H., and Baldwin, R. L. (1999) Specificity of native-like interhelical hydrophobic contacts in the apomyoglobin intermediate, *Proc. Natl. Acad. Sci. U.S.A. 96*, 2007−2012.
53. Gilmanshin, R., Callender, R. H., and Dyer, R. B. (1998) The core of apomyoglobin E-form folds at the diffusion limit, *Nat. Struct. Biol. 5*, 363−365.
54. Gulotta, M., Gilmanshin, R., Buscher, T. C., Callender, R. H., and Dyer, R. B. (2001) Core formation in apomyoglobin: probing the upper reaches of the folding energy landscape, *Biochemistry 40*, 5137−5143.
55. Kubelka, J., Hofrichter, J. and Eaton, W. A. (2004) The protein folding 'speed limit', *Curr. Opin. Struct. Biol. 14*, 76−88.

BI047372V